ARTICLE

ACS chemical biology

Imaging Distinct Conformational States of Amyloid-β Fibrils in Alzheimer's Disease Using Novel Luminescent Probes

K. Peter R. Nilsson[†,], Andreas Åslund[†], Ina Berg[†], Sofie Nyström[†], Peter Konradsson[†], Anna Herland[‡], Olle Inganäs[‡], Frantz Stabo-Eeg[§], Mikael Lindgren[§], Gunilla T. Westermark[¶], Lars Lannfelt[∥], Lars N. G. Nilsson[∥], and Per Hammarström[†,*]**

[†]IFM-Department of Chemistry, Linköping University, SE-581 83 Linköping, Sweden, [‡]Biomolecular and Organic Electronics, IFM, Linköping University, SE-581 83 Linköping, Sweden, [§]Department of Physics, The Norwegian University of Science and Technology, 7491 Trondheim, Norway, [¶]Division of Cell Biology, Linköping University, SE-581 83 Linköping, Sweden, and [∥]Department of Public Health and Caring Sciences, Rudbeck Laboratory, Uppsala University, Dag Hammarskjölds Väg 20, SE-751 85 Uppsala, Sweden., **Present address: UniversitätsSpital Zürich, Institute of Neuropathology, Schmelzbergstrasse 12, CH-809 Zürich, Switzerland.

ABSTRACT Using luminescent conjugated polyelectrolyte probes (LCPs), we demonstrate the possibility to distinguish amyloid-β 1–42 peptide (Aβ1–42) fibril conformations, by analyzing *in vitro* generated amyloid fibrils of Aβ1–42 formed under quiescent and agitated conditions. LCPs were then shown to resolve such conformational heterogeneity of amyloid deposits *in vivo*. A diversity of amyloid deposits depending upon morphology and anatomic location was illustrated with LCPs in frozen *ex vivo* brain sections from a transgenic mouse model (tg-APP_{swe}) of Alzheimer's disease. Comparative LCP fluorescence showed that compact-core plaques of amyloid β precursor protein transgenic mice were composed of rigid dense amyloid. A more abundant form of amyloid plaque displayed morphology of a compact center with a protruding diffuse exterior. Surprisingly, the compact center of these plaques showed disordered conformations of the fibrils, and the exterior was composed of rigid amyloid protruding from the disordered center. This type of plaque appears to grow from more loosely assembled regions toward solidified amyloid tentacles. This work demonstrates how application of LCPs can prove helpful to monitor aggregate structure of *in vivo* formed amyloid deposits such as architecture, maturity, and origin.

Accumulation of amyloid plaques in the hippocampus and cerebral cortex of the brain is a pathological hallmark of Alzheimer's disease (AD). Senile plaques in AD display several different microscopic morphologies, including compact-core plaque, compact plaque with diffuse exterior, and diffuse deposits, often with a "cotton wool" appearance (*1, 2*). It has recently become evident that it is not only the mature amyloid fibrils that are the toxic species but also intermediates along or off the amyloid assembly pathway that can execute deleterious effects (*3–6*). Several questions still remain regarding the molecular mechanism of aggregation into oligomeric and fibrillar structures, the dynamic interplay between these species, and the pathogenic information encoded in multiple conformations and morphologies, of amyloid deposits.

Luminescent conjugated polyelectrolyte probes (LCPs) can be used as amyloid-specific dyes for staining of amyloid-containing tissue and work as conformationally sensitive probes for the detection of amyloid fibril formation *in vitro* (*7–9*). In contrast to sterically rigid amyloidotropic dyes such as thioflavin T (ThT) (*10*) and Congo red (*11*), LCPs have a flexible thiophene backbone, which provides a correlation between the conformation of the probe and the spectral characteristic of that particular conformation. Noncovalent binding of LCPs to proteins in different conformations constrains the rotational freedom of LCPs, affording a spectroscopic signature for individual protein conformations (*7–9*).

*Corresponding author, perha@ifm.liu.se.

Received for review May 25, 2007 and accepted July 9, 2007.

Published online August 3, 2007

10.1021/cb700116u CCC: $37.00

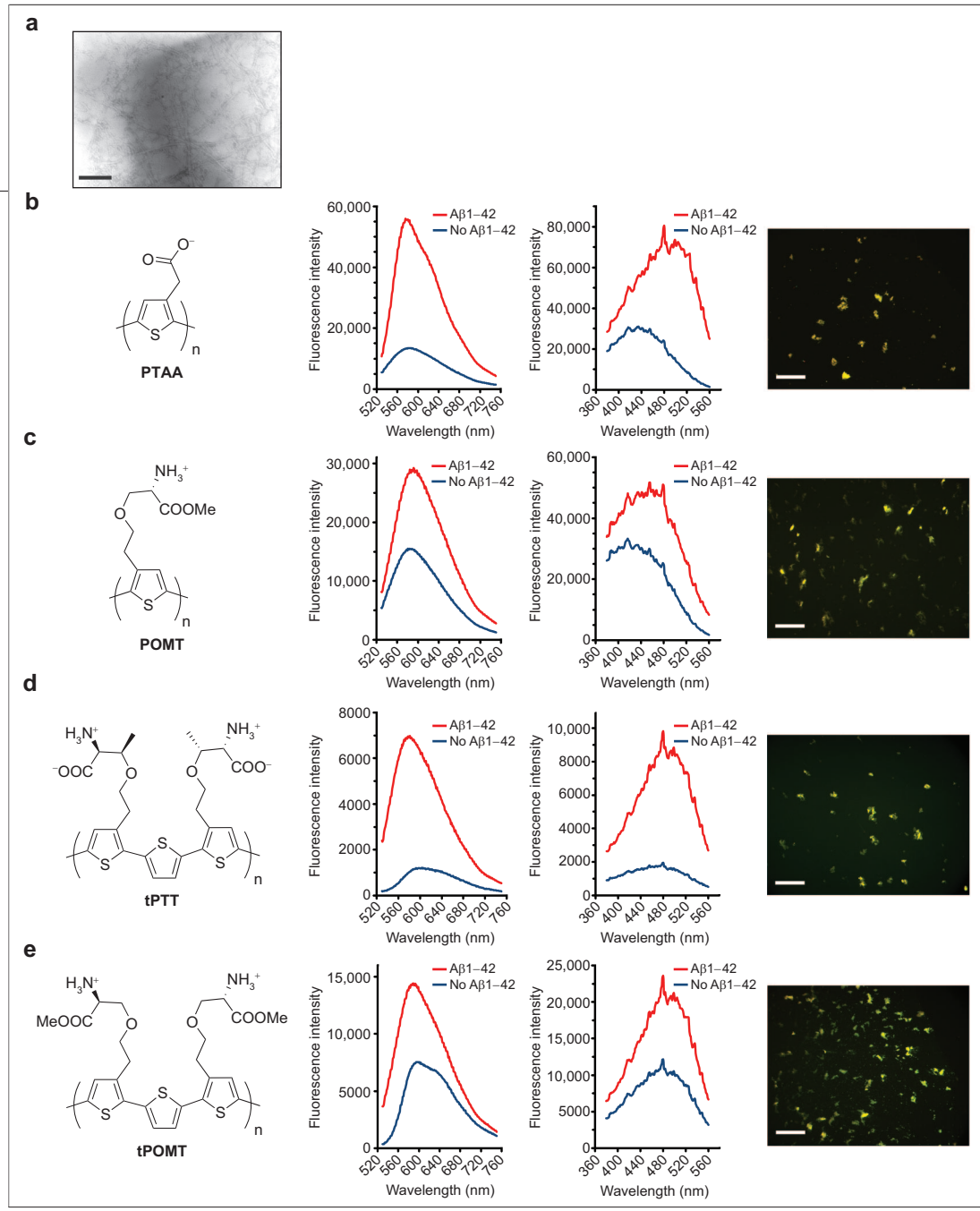

Figure 1. LCP binding of Aβ1–42 amyloid fibrils *in vitro*. a) Electron micrograph of amyloid fibrils of Aβ1–42 generated *in vitro* by quiescent incubation 50 μM Aβ1–42 (50 mM Tris-HCl, pH 7.5) for 5 d at 37 °C. Scale bar represents 200 nm. b) PTAA, c) POMT, d) tPTT, and e) tPOMT fluorescence emission (left) and excitation spectra (right) in the presence and absence of Aβ1–42 amyloid. The far right panel in panels b–e shows fluorescence micrographs of pelleted Aβ1–42 amyloid fibrils stained with the respective LCPs. Micrographs were recorded using a Zeiss Axiovert inverted microscope A200 Mot equipped with a CCD camera (Axiocam HR), using a 470/40 nm bandpass filter (LP515) and a 546/12 nm bandpass filter (LP590). Scale bars represents 200 μm. Emission spectra were obtained following 488 nm excitation wavelength, and emission spectra were recorded using 600 nm emission wavelength.

RESULTS AND DISCUSSION

Amyloid fibrils of amyloid-β 1–42 peptide (Aβ1–42) generated *in vitro* and *in vivo* were analyzed using four different LCPs. Analyses were performed using spectroscopy, microscopy, and spectrally resolved microscopy. Heterogeneities of amyloid depositions *in vivo* were simulated *in vitro*. Fibril morphology of *in vitro* fibrils was analyzed using ultrastructural analysis by transmission electron microscopy (TEM) and atomic force microscopy (AFM).

Luminescence of LCPs Bound to Aβ1–42 Amyloid *in Vitro*. Initially, three different LCPs with similar polythiophene backbones but with distinct ionic side chain functionalities (Figure 1, panels b–d) were selected. Further-

more, poly(5,5′′)terthiophene-(*S*)-2-amino-3-(2-{3′′-[2-((*S*)-2-amino-2-methoxycarbonyl-ethoxy)-ethyl]-[2,2′;5′,2′′]terthiophen-3-yl}-ethoxy)-propionic acid methyl ester (tPOMT) represents a defined oliothiophene with the same side chain functionality as poly(3-[(*S*)-5-amino-5-carboxyl-3-oxapentyl]-2,5-thiophenylene hydrochloride (POMT). Hence, four LCPs—polythiophene acetic acid (PTAA, anionic), POMT (cationic), poly(5,5′′)tertiophene -(2*S*,3*R*)-2-amino-3-(2-{3′′-[2-((1*R*,2*S*)-2-amino-2-carboxy-1-methyl-ethoxy)-ethyl]-[2,2′;5′,2′′]terthiophen-3-yl} -ethoxy)-butyric acid (tPTT, zwitterionic), and tPOMT (cationic)—were investigated for luminescence response during binding to Aβ1–42 amyloid fibrils *in vitro*. The synthesis of PTAA and POMT has been published previously (*12, 13*) and the synthesis of tPTT and tPOMT is described here (Supplementary Scheme 1). Amyloid fibrils of Aβ1–42 were generated *in vitro* using a quiescent incubation setup (50 μM Aβ1–42; 50 mM Tris-HCl, pH 7.5, 37 °C, for 5 d). Formation of amyloid fibrils was verified by ThT binding (data not shown) and TEM (Figure 1, panel a). Emission and excitation fluorescence spectra of free LCP and LCP bound to Aβ1–42 amyloid fibrils were obtained (Figure 1, panels b–e). Emission spectra showed increased quantum yield for all LCPs bound to Aβ1–42 amyloid fibrils. The excitation spectra revealed an augmented fluorescence response and a dramatic spectral red shift for all LCPs, indicating that the probes bind in a stretched planar conformation to the amyloid fibrils. Stained amyloid fibrils were also visualized by fluorescence microscopy, revealing large aggregates of bundled amyloid fibrils (Figure 1, panels b–e, right panel).

Histological LCP Staining of AD Brains. The LCP technology was demonstrated to enable conformational mapping of individual plaques formed in brains of transgenic mice harboring the Swedish mutations K670N/M671L in the amyloid-β precursor protein (APP) gene (tg-APP_{Swe}). In tg-APP_{Swe} mice, a transgenic model of AD amyloidosis, APP harboring the Swedish mutation (K670M/N671L) is overexpressed in neurons (*14–16*). A small amount of intraneuronal Aβ aggregates can be seen at 7 mo, while core plaque as well as cerebrovascular amyloid start to appear at around 12 mo of age and continue to accumulate over time. This age-dependent plaque formation in the hippocampus and the cerebral cortex of the tg-APP_{Swe} mouse makes it an attractive tool for studies of amyloid composition and propagation of Aβ amyloidosis (*14*). Mildly fixed (70% cold ethanol) brain cryostat sections from a tg-APP_{Swe} mouse aged 18 mo were stained with Congo red, ThT, and PTAA to verify amyloid specificity. Extracellular amyloid was extensive at 18 mo (*14*). Core plaque and vascular amyloid were strongly fluorescent after staining with PTAA (Supplementary Figure 1, panel a), ThT (Supplementary Figure 1, panel b), or Congo red (Supplementary Figure 1, panel c). There was excellent agreement between structures recognized by the LCPs and the conventional amyloidotrophic dyes. All four LCPs visualize amyloid plaques in the cortex using multiple fluorescence wide bandpass filters suitable for investigating the broad spectral distribution of the LCP in different conformations (Figure 2, panels c–f). The plaques detected by the LCPs were confirmed to be Aβ by immunolabeling with the 6E10 antibody on consecutive sections (Figure 2, panel a) and large plaques were amyloid-positive by ThT fluorescence (Figure 2, panel b). Close examination of the LCP-stained plaques revealed a variety in luminescence hue, especially for tPTT and to some extent for PTAA. Several types of plaques could be defined in tissue sections from both the cortex and the hippocampus stained with tPTT (Figure 3, panels a and b; Figure 4, panels a and b; Supplementary Figure 2). Extracellular amyloid formation in the tg-

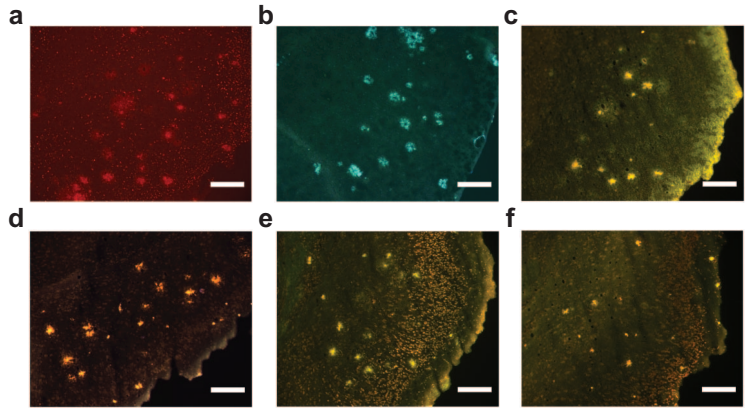

Figure 2. Histological staining in the cerebral cortex of an 18 mo tg-APP_{Swe} mouse. a) Immunofluorescence (6E10 antibody) (546 nm filter). Intense staining of Aβ shows as punctate fluorescence. Large amounts of bulky plaques appear throughout the cortex. b) ThT staining (distilled water) (405/470 nm filters). c) PTAA staining (pH 10) showing intense yellow appearance of plaques (470/546 nm double filter). d) POMT staining (pH 1) showing intense orange appearance of plaques (405/470/546 nm filters). e) tPTT staining (pH 1) (470/546 nm double filter). f) tPOMT staining (pH 1) (470/546 nm double filter). The scale bars indicate 200 μm.

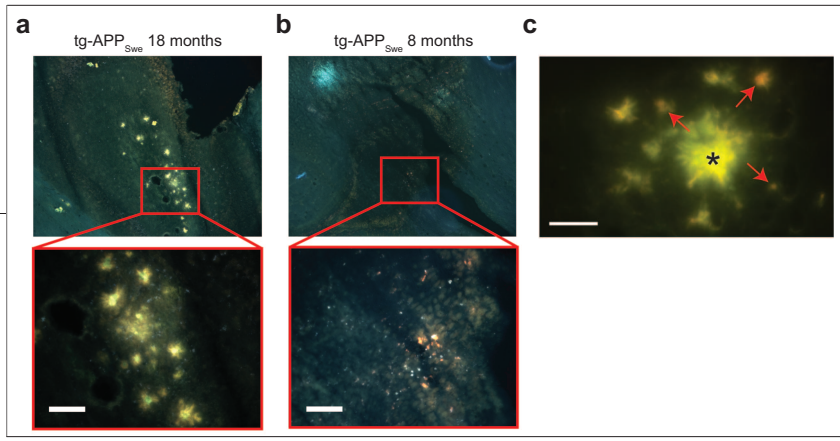

Figure 3. LCP staining of sectioned brains from tg-APP$_{Swe}$ mice at different ages. a) Histological staining of hippocampus of an 18 mo tg-APP$_{Swe}$ mouse with tPTT (405 nm filter). Large amounts of widely spread compact plaques with diffuse exterior and diffuse deposits appear throughout the dentate gyrus of the inner hippocampus. The central regions of the plaques fluoresce in green and the peripheral parts in orange. b) Histological staining of hippocampus of an 8 mo tg-APP$_{Swe}$ mouse with tPTT (405 nm filter) showing the lack of widespread plaque formation but formation of small microplaques that intensely fluoresce in orange. c) Histological staining of a core plaque in the cerebral cortex of an 18 mo tg-APP$_{Swe}$ mouse by PTAA (470/546 nm filters). The large patchy central compact plaque with diffuse exterior (*) fluoresces with a center ranging from yellow to green with the exterior shifting toward orange. Small peripheral plaques in the vicinity of the large plaque fluoresce in orange (indicated with red arrows). The scale bars indicate 50 μm.

APP$_{Swe}$ mouse model was very sparse at 8 mo of age; however close examination of tPTT, stained brain reveal small portions of microplaque in the dentate gyrus of the hippocampus (Figure 3, panel b). These plaques fluoresce intensely in orange as a result of densely packed LCP chains with extended conformation imposed by binding to compact amyloid in these microplaques. Very similar microplaques with analogous fluorescence properties were previously found in the cortex of human AD brain stained with PTAA (*8*). Mature compact-core plaques also fluoresce with an intense orange color (Figure 4, panel b), suggesting that the dense microplaques can be the origin of this type of mature plaques, which share the same LCP signal profile. A minority of plaques with the star-shaped compact plaque with diffuse exterior morphology show an orange fluorescent core. However, the majority of the compact plaques with diffuse exterior uncovered an orange colored periphery and a green center (Figure 3, panel a; Figure 4, panels a and b). The diffuse deposits localized adjacent to these plaques also fluoresced in orange (Figure 3, panel a; Figure 4, panel a). The red-shifted fluorescence of the periphery is indicative of planar and closely assembled tPTT probes. In contrast, the green emission of the center of these plaques indicates more twisted LCP chains with a lower amount of interchain aggregation. PTAA could also discriminate different plaque structures. PTAA visualized both small orange fluorescent compact-core plaques and compact plaques with diffuse exteriors, which fluoresced with a yellow/green center and an orange glowing exterior (Figure 3, panel c). Taken together, the data implied that the diffuse-appearing exterior from the large plaques buds off to seed initiation of surrounding small plaques.

Spectrally Resolved Confocal Microscopy of Individual Amyloid Plaques. To verify the obtained visual color emission with photophysical characteristics, we employed confocal microscopy with spectral resolution, enabling spectra to be collected from different areas of a tissue section (Figure 4, panel c). Spectra recorded from peripheral parts of individual plaques show a stronger emission in the red region compared with those recorded from the plaque center (Figure 4, panel d). A ratio plot of the emission enables a catalog of the physical properties of the bound tPTT, reporting on its conformation and packing. The green emission derives from twisted and separated LCP chains that fluoresce most intensely in the 543–564 nm region, and planar closely stacked chains fluoresce in the red spectral region at 639–661 nm. A bar graph of the fluorescence spectra of the periphery and of the center of individual plaques reveals that the periphery was shifted toward red fluorescence compared with the center. This indicates that the exterior of amyloid plaque is made up by tightly packed Aβ in amyloid fibril cross-β-sheet, whereas the center appears more loosely packed, detected as green fluorescence, a sign of twisted LCP chains with a lower degree of interchain packing.

Discrimination of Aβ1–42 Conformational Isoforms. To validate that the observed variability in LCP emission is associated with distinct conformational isoforms of Aβ-fibrils, we employed tPTT staining of Aβ1–42 amyloid-like fibrils grown *in vitro* under quiescent or agitated conditions. These conditions have previously been shown by the Tycko group (*17*) to induce distinctly folded isoforms of Aβ1–40. Ultrastructural analysis by TEM and AFM showed that Aβ1–42 fibrils grown under quiescent conditions were composed of separate elongated twisted fibrils (Figure 1, panel a; Figure 5, panels a and b). AFM analysis provided three different fibril thicknesses of 8.0 ± 0.8 nm, 12.7 ± 2.6 nm, and 22.7 ± 1.5 nm (Supplementary Figure 3) with an average fibril length of 0.72 ± 0.43 μm. Aβ1–42 fibrils grown under agitated conditions were structurally different, where TEM showed weblike structures of clustered fibrils (Figure 5, panel d). AFM analysis of separate fibrils

(Figure 5, panel e) revealed two different fibril thicknesses of 8.2 ± 1.0 nm and 12.0 ± 1.1 nm (Supplementary Figure 3) with an average fibril length of 0.27 ± 0.1 μm. Hence, the comparison showed that quiescent fibrils were more separated, twisted, more well defined, longer, and composed of a significant fraction of wider fibrils than fibrils of Aβ1−42 formed under agitation. Fluorescence micrographs of tPTT-stained fibrils of each type showed a distinctive color difference where the quiescent fibrils were orange and the agitated fibrils fluoresced in green (Figure 5, panels c and f). Collated emission spectra from several aggregates of each type verify that the color dissimilarity is a true spectroscopic difference (Figure 5, panel g). The green/red emission ratio analysis (Figure 5, panel h) shows that tPTT distinguished these fibril morphologies likely reflecting different conformational isoforms of Aβ1−42 and reported that quiescent fibrils have a more straight morphology and the agitated fibrils are more disordered, well in accordance with the ultrastructural analysis. Notably, a ThT assay from both types of fibrils was indistinguishable, but tPTT fluorescence in the same experimental setup was distinctly different (Figure 5, panel i).

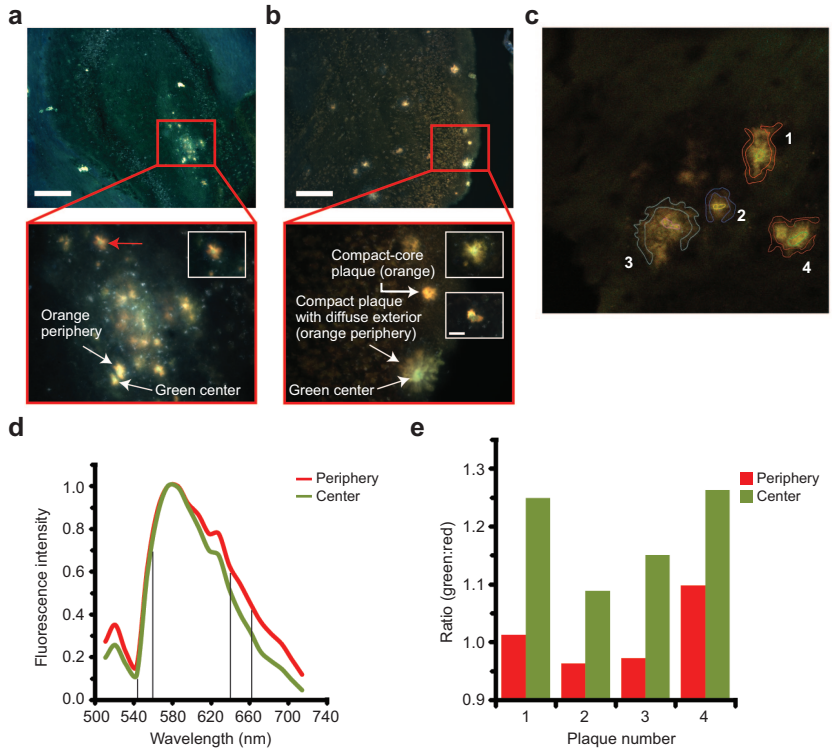

Figure 4. Conformational heterogeneity of amyloid plaques in tPTT-stained 18 mo tg-APP$_{Swe}$ mouse brain. a) Fluorescence microscope image showing localized distribution of amyloid plaques in the dentate gyrus of the hippocampus. A close-up reveals differential color of the compact plaques with diffuse exteriors showing orange fluorescence of the plaque periphery and green fluorescence of the plaque core indicated in the image with white arrows. The plaque indicated with a red arrow is enlarged in the inset. b) Fluorescence microscope image showing localized distribution of amyloid plaques in the cerebral cortex. The compact plaques with diffuse exteriors show an orange periphery and a green center as indicated with arrows. In addition, a compact core plaque showing intense orange fluorescence is also visible. The insets show high magnification images of plaques from independently stained tissue sections with green centers and orange exteriors. Scale bar of the upper micrograph represents 200 μm and 20 μm for the inset images in the lower micrograph. c) Confocal microscope image of four compact plaques with diffuse exterior in the cerebral cortex, where regions of the periphery and center were selected for spectral analysis as indicated with colored lines. d) Normalized fluorescence spectra from the periphery and center of plaque 1 indicated in panel c. The green (range between 543 and 564 nm) and red (range between 639 and 661 nm) spectral components are indicated. e) Bar plot of the ratio of the fluorescence intensity of the green component (integrated between 543 and 564 nm) and the red component (integrated between 639 and 661 nm) of the spectra from the individual plaques 1−4 in panel c. For all plaques, the periphery shows a larger red contribution than the center.

Concluding Remarks. The compact plaque with diffuse exterior appears to form from a disordered center with growing solidified amyloid tentacles protruding from the core. But the alternate possibility cannot be excluded, that rigid amyloid fibrils assemble and generate a plaque that grows from the outside in, forming a distorted center region where complete rigid structures have not yet matured. Importantly, very similar conclusions about the organization amyloid plaques as reported here have been reported previously from polarization microscopy of Congo red-stained plaques from human brains (*18*). Our data validate these earlier results. It has been shown that plaque formation can be seeded through inoculation with AD brain homogenate (*19, 20*). A combination of LCP staining and seeding experiments could enable resolution of these two models of plaque growth. The amyloid-spreading mechanism in different amyloidoses is unexplored territory, but insight into this mechanism would be instrumental for the understanding of amyloid toxicity and infectivity (*21, 22*) and likely for prion replication (*23*). We propose that the LCP conformational analysis can scout amyloid-spreading pathways and add knowl-

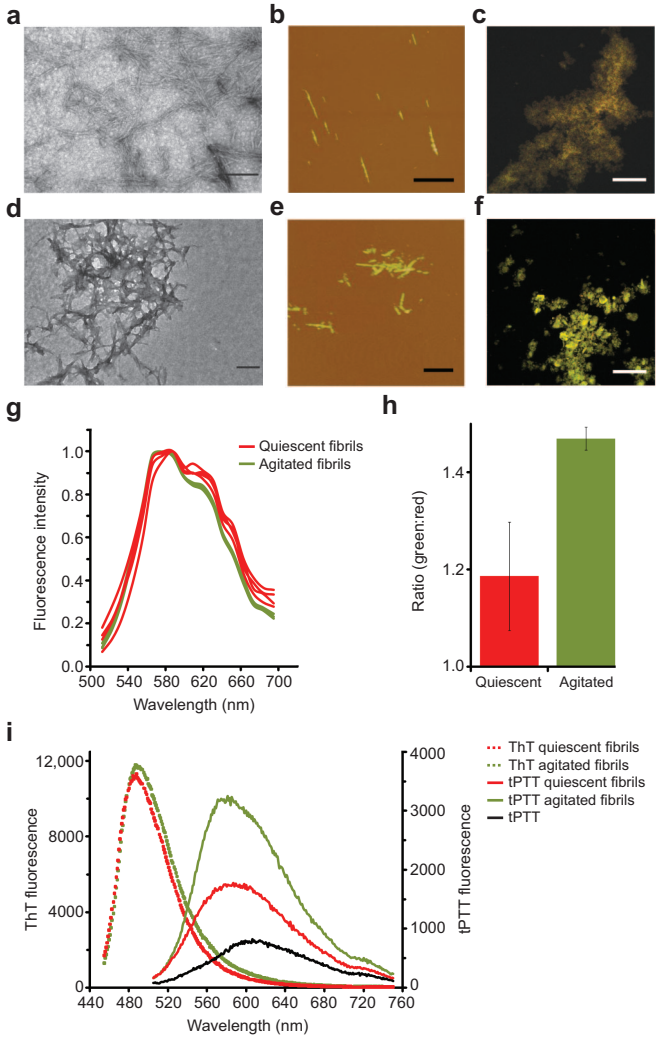

Figure 5. Conformational discrimination of *in vitro* Aβ1–42 amyloid fibrils. Fibrils grown under quiescent (panels a–c) and agitated conditions (panels d–f) were analyzed by TEM, AFM, and LCP fluorescence. a, d) Ultrastructural analysis by TEM scale bars are 0.2 μm. b, e) Ultrastructural analysis by AFM; scale bars are 0.2 μm in panel a and 500 nm in panel e. c, f) Confocal micrographs of pelleted fibrils stained with tPTT. Scale bars 50 μm. g) Average fluorescence spectra from confocal micrographs recorded with a META detector of three regions of interest from four different aggregates of quiescent fibrils and three different aggregates of agitated fibrils. h) Bar plot of the ratio of the fluorescence intensity of the green and red components as described in the Methods section (and legend to Figure 4, panel e). The quiescent fibrils show a larger red emission component compared with the agitated fibrils. i) ThT fluorescence and tPTT fluorescence of agitated and quiescent Aβ1–42 amyloid fibrils in 50 mM Tris-HCl, pH 7.5.

edge to the amyloid cascade hypothesis (*24*) or prion propagation theory (*25*). In addition, the methodology presented here can likely be of use to image growth of pathogenic amyloid structures *in vivo*. We have previously shown that LCPs in multiphoton excitation opening the door for *in vivo* experiments using near IR wavelengths (*8, 26*) shown possible for other fluorescent dyes (*27*).

The optical fingerprint obtained from the LCPs that reflects the conformational differences in distinct protein aggregates is a unique property for the LCPs and is not offered by any of the commonly used amyloidotropic dyes. In this regard, LCPs could improve the precision of diagnoses of aggregation proteopathies and facilitate analysis of amyloid maturity and origin and discrimination of amyloid strains.

METHODS

LCPs. PTAA and POMT were synthesized as previously described (*12, 13*). tPTT and tPOMT were synthesized as described in Supplementary Scheme 1.

Histology. Tg-APP$_{swe}$ mice with 7-fold human APP overexpression were sacrificed at 8 and 18 mo. The generation and characterization of this APP transgenic model has been previously described (*14*). Brains were recovered, sliced, and snap-frozen in CO_2–pentane (−30 °C). Tissue from representative areas were mounted on a chuck, and 10 μm tissue sections were cut on a cryostat microtome. The sections were fixed for 10 min in 70% ethanol (4 °C).

The sections were equilibrated with 50 mM HCl (pH 1) or 50 mM sodium carbonate (pH 10) for 1 h and then incubated with 25 μg mL^{-1} PTAA, POMT, tPTT, or tPOMT for 2 h (21 °C) in a humidity chamber.

Consecutive sections were used for comparative staining of amyloid with PTAA, Congo red, and ThT. The sections were counterstained with Mayer's hematoxylin for 1 min and rinsed in tap water for 5 min. Congo red staining was performed in Congo red working solution (3 mg mL^{-1} Congo red dissolved in 80% ethanol containing 3 mg mL^{-1} NaCl and 0.001% (w/v) NaOH) for 10 min, followed by differentiation in alkaline ethanol and rinsing in water.

ThT staining was performed in 0.003 mg mL^{-1} ThT in distilled water for 5 min followed by differentiation in 70% ethanol for 5 min and rinsing in water.

Amyloid deposits were immunolabeled with the 6E10 monoclonal antibody (Signet laboratories) (dilution 1:1000). To prevent unspecific binding, the sections were incubated in 4% bovine serum albumin (MP Biomedicals Inc., cat no. 199757) dissolved in phosphate buffer with 0.2% Triton X-100 (BioRad, cat no. 161-0407) (PBT) for 2 h at RT. The primary antibody was diluted 1:250 in the same buffer, and the sections were incubated overnight at 20 °C. The sections were rinsed in PBT, and the 6E10 antibody was detected by incubation in Rhodamine Red-X-conjugated AffinitiPure Donkey Anti-Mouse IgG (H+L) (Jackson Immuno Research Laboratories Inc., cat no. 715-295-150) diluted 1:250 for 30 min at RT. Thereafter, the sections

were rinsed in PBT and mounted with Vectashield mounting solution for fluorescence (Vector Laboratories Inc., cat no. R0328).

Fluorescence Spectroscopy of *in Vitro* Aβ1−42 Amyloid Fibrils. *In vitro* Aβ1−42 amyloid fibrils were prepared by solubilization of recombinant Aβ1−42 (rPeptide) (50 μM) in 50 mM Tris-HCl (pH 7.5) and incubation for 5 d at 37 °C. The fibrils were poured into a dialysis membrane (3500 MW) and were dialyzed against dH_2O overnight (4 °C). Prepared samples contain 12.5 μM Aβ1−42 fibrils with 4 μM LCP (in 50 mM HCl (pH 1) for POMT, tPTT, and tPOMT and in 50 mM sodium carbonate (pH 10) for PTAA). Reference spectra were obtained of 4 μM LCP alone under identical conditions. For comparative studies between quiescent and agitated Aβ1−42 amyloid fibrils, the same conditions for fibril growth as above were employed, but Aβ1−42 samples were only incubated for 48 h. The fibrils were then directly mixed (no dialysis) with tPTT (or ThT) in 50 mM Tris-HCl, pH 7.5. Excitation and emission fluorescence spectra were obtained using a Tecan Infinity and a Tecan Saphire2 fluorescence plate reader.

TEM and AFM. Aβ1−42 amyloid fibril suspension (5 μL) from recombinant Aβ1−42 was placed on a carbon-coated copper grid (Carbon B, Ted Pella Inc.) for 2 min, and the excess was was blotted dry with a filter paper. One round of rinsing was performed with 5 μL of dH_2O. The sample was thereafter stained using 2% (w/v) uranyl acetate dissolved in water for 20 s and blotted dry, and the grids were dried overnight. The fibril morphology was evaluated in a Philips CM200 transmission electron microscope operating at 120 kV and with a Philips CM20 ST operating at 200 kV. AFM imaging was performed in tapping mode on a SFM-Nanoscope III, Digital Instruments, with a J-scanner. For the AFM observations, 3 μL of fibril suspension (diluted 10× with water) was applied to a hydrophobic silicon (100) surface coated with a monolayer of dichlorodimethylsilane and incubated for 2 min, and excess protein was removed by extensive rinsing in deionized water followed by drying using pressurized N_2.

Fluorescence Microscopy. Tissues samples and LCP stained *in vitro* generated fibrils (pelleted at 10,000*g* for 30 min) were recorded with an epifluorescence microscope (Zeiss Axiovert inverted microscope A200 Mot) equipped with a CCD camera (Axiocam HR), using a 405/30 nm bandpass filter (LP450), a 470/40 nm bandpass filter (LP515), and a 546/12 nm bandpass filter (LP590).

Spectrally Resolved Confocal Microscopy. Confocal fluorescence imaging of tissue sections was performed using an LSM 510 META (Carl Zeiss, Jena, Germany) confocal laser scanning microscope with Plan-Neofluar 10×/0.3, 20×/0.5, and 40×/0.75 objectives, using an argon 488 nm laser for excitation. The ratio of the green and red components in the spectra was calculated from the formula: $\sum^{564}_{543}/\sum^{661}_{639}$, indicating the ratio of the integrated emission from tPTT in the region between 543 and 564 nm and between 639 and 661 nm.

Acknowledgment: This work was funded by grants from the Swedish Foundation for Strategic Research (P.H.), Knut and Alice Wallenberg Foundation (K.P.R.N., P.H.), grants from Uppsala University (L.L.), Landstinget i Uppsala län (L.L.), the Swedish Brain Fund following a donation by Bertil Hållstens Forskningsstiftelse (L.L.), Alzheimerfonden (L.L.), Gamla Tjänarinnor (L.N.), Stohnes (L.N.), Magnus Bergvall (L.N.), Åhlénsstiftelsen (L.N.), Lars Hierta (L.N.), Lundströms Minne (L.N.), Frimurarstiftelsen (L.N.), Läkarsällskapet (L.N.), the Swedish Research Council (P.H. (No. 2004-2696); O.I. (No. 2005-5156); L.L. (No. 2006-2822); L.N. (No. 2006-2818)), and the Norwegian Research Council within the NanoMat program (M.L., No. 153529/s10). The Uppsala University Transgenic Facility is greatly acknowledged for their help in developing the APP transgenic model used in this study, tg-APP_{Swe} mice.

Supporting Information Available: This material is free of charge *via* the Internet.

REFERENCES

1. Bussiere, T., Bard, F., Barbour, R., Grajeda, H., Guido, T., Khan, K., Schenk, D., Games, D., Seubert, P., and Buttini, M. (2004) Morphological characterization of thioflavin-S-positive amyloid plaques in transgenic Alzheimer mice and effect of passive Aβ immunotherapy on their clearance, *Am. J. Pathol. 165*, 987–995.
2. Ikonomovic, M. D., Abrahamson, E. E., Isanski, B. A., Debnath, M. L., Mathis, C. A., Dekosky, S. T., and Klunk, W. E. (2006) X-34 labeling of abnormal protein aggregates during the progression of Alzheimer's disease, *Methods Enzymol. 412*, 123–144.
3. Lambert, M. P., Barlow, A. K., Chromy, B. A., Edwards, C., Freed, R., Loisatos, M., Morgan, T. E., Rozovsky, I., Tromber, B., Viola, K. L., Wals, P., Zhang, C., Finch, C. E., and Krafft, G. A. (1998) Diffusible, nonfibrillar ligands derived from Abeta1−42 are potent central nervous system neurotoxins, *Proc. Natl. Acad. Sci. U.S.A. 95*, 6448−6453.
4. Bucciantini, M., Giannoni, E, Chiti, F., Baroni, F., Formigli, L., Zurdo, J., Taddei, N., Ramponi, G., Dobson, C.M., and Stefani, M. (2002) Inherent toxicity of aggregates implies a common mechanism for protein misfolding diseases, *Nature 416*, 507–511.
5. Bucciantini, M., Calloni, G., Chiti, F., Formigli, L., Nosi, D., Dobson, C. M., and Stefani, M. (2004) Prefibrillar amyloid protein aggregates share common features of cytotoxicity, *J. Biol. Chem. 30*, 31374−31382.
6. Baglioni, S., Casamenti, F., Bucciantini, M., Luheshi, L. M, Taddei, N., Chiti, F., Dobson, C.M., and Stefani, M. (2006) Prefibrillar amyloid aggregates could be generic toxins in higher organisms, *J. Neurosci. 26*, 8160−8167.
7. Nilsson, K. P. R., Herland, A., Hammarström, P., and Inganäs, O (2005) Conjugated polyelectrolytes: conformation-sensitive optical probes for detection of amyloid fibril formation, *Biochemistry 44*, 3718−3724.
8. Nilsson, K. P., Hammarström, P, Ahlgren, F., Herland, A., Schnell, E. A., Lindgren, M., Westermark, G. T., and Inganäs, O. (2006) Conjugated polyelectrolytes—conformation-sensitive optical probes for staining and characterization of amyloid deposits, *ChemBioChem 7*, 1096−1104.
9. Herland, A., Nilsson, K. P. R., Olsson, J. D. M., Hammarström, P., Konradsson, P., and Inganäs, O. (2005) Synthesis of a regioregular zwitterionic conjugated oligoelectrolyte, usable as an optical probe for detection of amyloid fibril formation at acidic pH, *J. Am. Chem. Soc. 127*, 2317−2323.
10. Naiki, H., Higuchi, K., Hosokawa, M., and Takeda, T. (1989) Fluorometric determination of amyloid fibrils *in vitro* using the fluorescent dye, thioflavin T1, *Anal. Biochem. 177*, 244−249.
11. Klunk, W. E., Pettegrew, J. W., and Abraham, D. J. (1989) Quantitative evaluation of congo red binding to amyloid-like proteins with a beta-pleated sheet conformation, *J. Histochem. Cytochem. 37*, 1273−1281.
12. Ding, L., Jonforsen, M., Roman, L. S., Andersson, M., and Inganäs, O. (2000) Photovoltaic cells with a conjugated poly electrolyte, *Synth. Met. 110*, 133−140.
13. Nilsson, K. P. R., Olsson, J. D. M., Stabo-Eeg, F., Lindgren, M., Konradsson, P., and Inganäs, O. (2005) Chiral recognition of a synthetic peptide using enantiomeric conjugated polyelectrolytes and optical spectroscopy, *Macromolecules 38*, 6813−6821.
14. Lord, A., Kalimo, H., Eckman, C., Zhang, X. Q., Lannfelt, L., and Nilsson, L. N. (2006) The Arctic Alzheimer mutation facilitates early intraneuronal Abeta aggregation and senile plaque formation in transgenic mice, *Neurobiol. Aging 27*, 67−77.
15. Stenh, C., Englund, H., Lord, A., Johansson, A.-S., Almeida, C. G., Gellerfors, P., Greengard, P., Gouras, G. K., Lannfelt, L., and Nilsson, L. N. G. (2005) Oligomers of amyloid-β are inefficiently measured by ELISA, *Ann. Neurol. 58*, 147−150.

16. Sahlin, C., Lord, A., Magnusson, K., Englund, H., Almeida, C. G., Greengard, P., Nyberg, F., Gouras, G. K., Lannfelt, L., and Nilsson, L. N. G. (2007) The Arctic Alzheimer mutation favors intracellular Aβ production by making APP less available to α-secretase, *J. Neurochem. 101*, 854–862.
17. Petkova, A. T., Leapman, R. D., Guo, Z., Yau, W. M., Mattson, M. P., and Tycko, R. (2005) Self-propagating, molecular-level polymorphism in Alzheimer's beta-amyloid fibrils, *Science 307*, 262–265.
18. Jin, L. W., Claborn, K. A., Kurimoto, M., Geday, M. A., Maezawa, I., Sohraby, F., Estrada, M., Kaminksy, W., and Kahr, B. (2003) Imaging linear birefringence and dichroism in cerebral amyloid pathologies, *Proc. Natl. Acad. Sci. U.S.A. 100*, 15294–15298.
19. Kane, M. D., Lipinski, W. J., Callahan, M. J., Bian, F., Durham, R. A, Schwarz, R. D., Roher, A. E., and Walker, L. C. (2000) Evidence for seeding of beta-amyloid by intracerebral infusion of Alzheimer brain extracts in beta-amyloid precursor protein-transgenic mice, *J. Neurosci. 20*, 3606–3611.
20. Meyer-Luehmann, M., Coomaraswamy, J., Bolmont, T., Kaeser, S., Schaefer, C., Kilger, E., Neuenschwander, A., Abramowski, D., Frey, P., Jaton, A. L., Vigouret, J. M., Paganetti, P, Walsh, D. M., Mathews, P. M., Ghiso, J., Staufenbiel, M., Walker, L. C., and Jucker, M. (2006) Exogenous induction of cerebral beta-amyloidogenesis is governed by agent and host, *Science, 313*, 1781–1784.
21. Lundmark, K., Westermark, G. T., Nystrom, S., Murphy, C. L., Solomon, A., and Westermark, P. (2002) Transmissibility of systemic amyloidosis by a prion-like mechanism, *Proc Natl Acad Sci U.S.A. 99*, 6979–6984.
22. Soto, C., Estrada, L., and Castilla, J. (2006) Amyloids, prions and the inherent infectious nature of misfolded protein aggregates, *Trends Biochem. Sci. 31*, 150–155.
23. Prusiner, S. B., McKinley, M. P., Bowman, K. A., Bolton, D. C., Bendheim, P. E., Groth, D. F., and Glenner, G. G. (1983) Scrapie prions aggregate to form amyloid-like birefringent rods, *Cell 35*, 349–358.
24. Hardy, J., and Higgins, G. (1992) Alzheimer's disease: the amyloid cascade hypothesis, *Science, 256*, 184–185.
25. Tanaka, M., Collins, S. R., Toyama, B. H., and Weissman, J. S. (2006) The physical basis of how prion conformations determine strain phenotypes, *Nature 442*, 585–589.
26. Stabo-Eeg, F., Lindgren, M., Nilsson K. P. R., Inganäs, O, and Hammarström, P. (2007) Quantum efficiency and two-photon absorption cross-section of conjugated polyelectrolytes used for protein conformation measurements with applications on amyloid structures, *Chem. Phys.*, in press, DOI :10.1016/j.chemphys.2007.06.020.
27. Hintersteiner, M., Enz, A., Frey, P., Jaton, A. L., Kinzy, W., Kneuer, R., Neumann, U., Rudin, M., Staufenbiel, M., Stoeckli, M., Wiederhold, K. H., and Gremlich, H. U. (2005) *In vivo* detection of amyloid-beta deposits by near-infrared imaging using an oxazine-derivative probe, *Nat. Biotechnol. 5*, 577–583.